Enhanced antitumor efficacy of biocompatible magnetosomes for the magnetic hyperthermia treatment of glioblastoma

Raphael Le Fèvre, Mickaël F Durand-Dubief, Imène F Chebbi, Chalani Mandawala, France Lagroix, Jean-Pierre Valet, Ahmed Idbaih, Clovis Adam, Jean-Yves Delattre, Charlotte Schmitt, et al.

IVYSPRING INTERNATIONAL PUBLISHER

Theranostics

2017; 7(18): 4618-4631. doi: 10.7150/thno.18927

Research Paper

Enhanced antitumor efficacy of biocompatible magnetosomes for the magnetic hyperthermia treatment of glioblastoma

Raphaël Le Fèvre[1, 2], Mickaël Durand-Dubief [1], Imène Chebbi[1], Chalani Mandawala[1, 3], France Lagroix[2], Jean-Pierre Valet[2], Ahmed Idbaih[5], Clovis Adam[6], Jean-Yves Delattre[5], Charlotte Schmitt[5], Caroline Maake[4], François Guyot[3], Edouard Alphandéry[1,3]✉

1. Nanobacterie SARL, 36 boulevard Flandrin, 75016, Paris.
2. Institut de Physique du Globe de Paris, Sorbonne Paris Cité, Univ. Paris Diderot, UMR 7154 CNRS, 1 rue Jussieu, 75005 Paris, France.
3. Institut de minéralogie de physique des matériaux et de cosmochimie, Sorbonne Université UMR 7590 CNRS, Université Pierre et Marie Curie, Muséum Naitonal d'Histoire Naturelle. 4 Place Jussieu, 75005, Paris, France.
4. Institute of Anatomy, UZH University of Zurich, Instiute of Anatomy, Winterthurerstrasse 190, CH-8057, Zurich, Switzerland.
5. Inserm U 1127, CNRS UMR 7225, Sorbonne Universités, UPMC, University Paris 06, UMR S 1127, Institut du Cerveau et de la Moelle épinière, ICM, F-75013, Paris, France. AP-HP, Hôpitaux Universitaires Pitié Salpêtrière - Charles Foix, Service de Neurologie 2-Mazarin, F-75013, Paris, France.
6. Laboratoire de neuropathologie, GHU Paris-Sud-Hôpital Bicêtre, 78 rue du Général Leclerc, 94270 Le Kremlin Bicêtre, France.

✉ Corresponding author: edouardalphandery@hotmail.com

Received: 2016.12.26; Accepted: 2017.10.04; Published: 2017.10.13

Abstract

In this study, biologically synthesized iron oxide nanoparticles, called magnetosomes, are made fully biocompatible by removing potentially toxic organic bacterial residues such as endotoxins at magnetosome mineral core surfaces and by coating such surface with poly-L-lysine, leading to magnetosomes-poly-L-lysine (M-PLL). M-PLL antitumor efficacy is compared with that of chemically synthesized iron oxide nanoparticles (IONPs) currently used for magnetic hyperthermia. M-PLL and IONPs are tested for the treatment of glioblastoma, a dreadful cancer, in which intratumor nanoparticle administration is clinically relevant, using a mouse allograft model of murine glioma (GL-261 cell line). A magnetic hyperthermia treatment protocol is proposed, in which nanoparticles yielding an amount of 25 of iron per mm^3 of tumor are administered and exposed to 11 to 15 magnetic sessions during which an alternating magnetic field of 198 kHz and 11 to 31 mT is applied for 30 minutes to attempt reaching temperatures of 43-46 °C. M-PLL are characterized by a larger specific absorption rate (SAR of 40 W/g_{Fe} compared to 26 W/g_{Fe} for IONPs as measured during the first magnetic session), a lower strength of the applied magnetic field required for reaching a target temperature of 43-46 °C (11 to 27 mT compared with 22 to 31 mT for IONPs), a lower number of mice re-administered (4 compared to 6 for IONPs), a longer residence time within tumours (5 days compared to 1 day for IONPs), and a less scattered distribution in the tumour. M-PLL lead to higher antitumor efficacy with full tumor disappearances achieved in 50% of mice compared to 20% for IONPs. This is ascribed to better ability of M-PLL, at equal iron concentrations, to maintain tumor temperatures at 43-46°C over a longer period of times.

Key words: Glioblastoma, nanomedicine, magnetic hyperthermia, alternating magnetic field, magnetotactic bacteria, magnetosomes

Introduction

Due to their low toxicity, iron oxide nanoparticles, IONPs, have been developed for different applications in diagnosis, *i.e.* as contrast agents in magnetic resonance imaging, MRI, or in

cancer treatment, using magnetic hyperthermia. In magnetic hyperthermia, magnetic nanoparticles are introduced to tumors and heated at 41-50 °C under the application of an alternating magnetic field (AMF) of 10-40 mT and 50-200 kHz, [1,2,3,4]. In such treatments, IONPs can be directly administered to glioblastoma of patients and heated under AMF application leading to an increased survival of 7 months compared with conventional treatments without inducing any major side effects, [5]. Other glioblastoma treatments, which currently use doxorubicin, temozolomide, lenalidomide oral administration, [6,7,8,9,10], lead to partial efficacy and often appear to be highly toxic, [11], necessitating the development of new treatments such as magnetic hyperthermia.

In this paper, we introduce new iron oxide nanoparticles, synthesized by magnetotactic bacteria, called magnetosomes, which are believed to be more efficient than chemical nanoparticles for magnetic hyperthermia treatments and can also be used for diagnostic purposes, [12,13,14,15]. This is due to a series of advantages such as improved heating properties, a high level of crystallinity, a specific homogenous distribution due to a chain arrangement. We have previously shown that it is possible to completely eradicate MDA-MB231 tumors of average volumes 100 mm^3 grown subcutaneously under the skin of mice by administering 1 mg of a suspension containing magnetosome chains at the centre of these tumors and by applying 3 times during 20 minutes an alternating magnetic field with a frequency of 183 kHz and strength of 40 mT, [16]. However, these encouraging results require further improvements. Indeed, chains of magnetosomes, which are directly extracted from gram negative magnetotactic bacteria without further treatment, contain endotoxins at their surface, which must be removed for medical applications. Moreover, these nanoparticles are synthetized by and extracted from AMB-1 magnetotactic bacteria, a strain of magnetotactic bacteria with a poor yield of magnetosome production of less than 200-400 µg of magnetosomes per litre of growth medium. It is necessary to improve this yield for medical applications, [17].

The new magnetosome synthesis method proposed herein increases the magnetosome production yield by a factor of 150 by using the MSR-1 instead of the AMB-1 strain, leading to the production of 120 mg of magnetosomes per litre of growth medium. Based on previous study, [5], it appears that 0.5 g of magnetosomes per patient may be necessary to treat glioblastoma using magnetic hyperthermia. Following a further step of up-scaling in larger volumes, which seems feasible and relatively inexpensive, [18], our treatment may be used at a large scale. The new method also eradicates the problem of endotoxins. Following extraction of magnetosomes from MSR-1 magnetotactic bacteria, magnetosomes are first purified to remove most organic material, and then coated with poly-L-lysine, to lead a biocompatible and stable suspension of magnetosome minerals coated with poly-L-lysine designated M-PLL. Anti-tumor efficacy of M-PLL and IONPs are compared by administering suspensions containing 25 µg in iron per mm^3 of tumor of M-PLL or IONPs at the centre of highly aggressive GL-261 glioblastoma tumors with sizes of 50 to 150 mm^3 grown subcutaneously on immunocompetent C57BL6 mice. Mice are then exposed to 11 to 15 magnetic sessions of 30 minutes during which an AMF operating at a frequency of 198 kHz and average strength regulated between 11 mT and 31 mT is applied to attempt maintaining intratumor temperature at 43-46 °C. These targeted temperatures are chosen since they lead to efficient magnetic hyperthermia treatment of various cancers (glioma, lymphoma, melanoma and carcinoma) without causing serious damage in healthy surrounding tissues, [19,20,21,22]. Comparison between M-PLL and IONPs efficacy is carried out, [23,24,25], by taking into consideration the strength of the magnetic field needed to reach an intratumor temperature of 43-46 °C, the number of mice requiring a second nanoparticle administration to re-activate the treatment, nanoparticle and temperature intratumor distributions, the decrease in tumor volume following treatments, and the percentage of fully cured mice.

Materials and Methods

Culture of magnetotactic bacteria in 70l semi-automated fermenter

Magnetospirillum gryphiswaldense strain MSR-1 (DSM6361) was purchased from Deutsche Sammlung von Mikro-organismen und Zellkulturen (Brunswick, Germany) and stored in small aliquots of 1 mL at - 80 °C. Cells were grown at 29 °C on solid activated charcoal agar medium as previously described, [26] under microaerobic conditions during 7 days. Several black-brown colonies were collected from the solid agar medium and amplified at 29 °C under stirring at 100 rpm in 10 L of a growth medium devoid of iron, [27]. Cells were then diluted in a 35 L fermentation medium also devoid of iron. Fermentation was carried out at 29-30 °C under agitation at 200 rpm during 5 days with pH maintained at 6.9 by adding an acidic feeding medium containing $FeCl_3.6H_2O$ as the iron source. Growth of magnetotactic bacteria was stimulated by bubbling oxygen in the growth medium at a percentage kept below 0.1 % to enable magnetosome synthesis, [28,29,30]. Temperature, agitation speed,

pH, feeding pump flow and oxygen concentration were monitored and adjusted using an EZ controller and a BioXpert software from Applikon Biotechnology.

Purification of uncoated magnetosome minerals

Following fermentation, MSR-1 cells were washed and concentrated in water using tangential flow filtration to an OD_{565} ~ 100. To lyse the bacteria, approximately 100 mL of concentrate MSR-1 cells were re-suspended in 400 mL of 1M NaOH and heated to 60 °C for 2 hours in 500 mL glass bottles placed in a sonicating bath at 25 kHz. A direct current field was then applied to the suspension overnight to separate magnetosomes from organic material residues. After separation, magnetosomes were re-suspended successively in: first, 500 mL of 1**x** PBS and sonicated at 10 W for 20 seconds, second 80 mL of 1% Triton X-100 and 1% SDS heated at 50 °C overnight, third 80 mL of phenol at pH 8 heated at 60 °C during 2 hours in the sonicating bath, fourth 80 mL of chloroform heated at 60 °C during 2 hours, and fifth 80 mL of 1 M NaOH solution heated at 60 °C for 1 hour in the sonicating bath. Between each step 1 to 5, magnetosome minerals were isolated from non-magnetic organic debris using a Neodymium magnet for 20 minutes. The supernatant was then removed and replaced by the next detergent or nonpyrogenic water after the fifth step. The resulting magnetosome minerals were autoclaved and stored at -80°C.

Coating of magnetosome minerals with poly-L-lysine

Uncoated magnetosome minerals were coated with PLL under sterile conditions. A suspension of PLL of 40 mg/ml (Gmac, CAS: 25988-63-0; molecular weight 21000 g/mol) mixed in pyrogen-free water was prepared, filtered with a polyethersulfone filter of 0.45 µm and stored at -80 °C. For the coating, seven times more PLL than magnetosome minerals in weight were used. A suspension containing 25 mL of magnetosome minerals (iron concentration of 3 mg/ml) was exposed to a 1.3 T magnetic field of a Neodymium magnet, the supernatant was replaced by 25 ml of PLL and the resulting suspension was introduced into a tube sonicated for 6 minutes at 4 °C using a 10 W sonicating finger. The tube was then shaken for 24 hours at 25 °C on a wheel, at a speed of 13 rpm and the suspension was sonicated again with a 10 W sonicating finger for 10 seconds at a temperature of 4-8 °C. Washing was carried out 1-4 times by placing the tube against the magnet, and by replacing the supernatant with sterile MilliQ water. The final suspension was sonicated for 2 minutes at 24 W on ice, holding the temperature below 4 °C to avoid heating, and the pH was adjusted to 6.8-7.2 with filtered KOH. We obtained a suspension of magnetosome minerals coated with PLL, herein referred to as M-PLL.

Preparation and characterization of IONPs

IONPs were purchased from Micromod Partikeltechnologie GmbH company, Germany (ref: 10-00-102). IONPs are starch coated iron oxide nanoparticles, which have previously been successfully used preclinically in the magnetic hyperthermia treatment of tumor, [31,33,33].

Characterization

The sizes and shapes of magnetosomes inside MSR-1 bacteria, magnetosome minerals, M-PLL and IONPs were observed using a transmission electron microscope (JEM-2100, JEOL, Japan). The iron concentration of the different suspensions containing magnetosome minerals, M-PLL or IONPs, were determined by a colorimetric test : nanoparticles were mixed with hydrochloric acid and hydrogen peroxide to produce Fe^{3+} ions complexed with potassium thiocyanate, and total iron was then determined by measuring the absorbance at 476 nm with a spectrophotometer (UviLine9400, SECOMAM, France). Zeta potential of the different nanoparticles in suspension was measured by Dynamic light scattering, DLS (ZEN 3600, Malvern Instruments, UK). The stability of these suspensions was determined by measuring variation of the optical density at 476 nm during 15 min with a spectrophotometer (UviLine9400, SECOMAM, France). Nanoparticle FTIR spectra were recorded with a FTIR spectrometer (Vertex 70, Bruker, USA). The amount of organic material at nanoparticle surface was measured using an elemental CHNS analyser (Flash EA 1112, Thermo Fisher Scientific, USA). Hysteresis loops of the different nanoparticles were measured at room temperature between -1 and +1 T using a vibrating sample magnetometer (VSM 3900, Princeton Measurements Corporation, USA). A Magnetic Properties Measurement System (MPMS XL-5, Quantum Design, USA) was used for saturating isothermal remanent magnetization (SIRM) measurements. More details about each of these techniques are provided in the supplementary material section.

Ethics statement

The *in vivo* study protocol was approved by the local animal ethics committee of the University Pierre-et-Marie-Curie (Paris, France).

Hyperthermia treatments

The GL-261 mouse glioma cell line (ATCC, USA) was cultivated in RPMI 1640 medium (GE Healthcare HyClone™, USA), supplemented with 10 % FBS at 37 °C in humidified atmosphere containing 5 % CO_2. About 10^7 cells in 100 µL RPMI with 0,1 % BSA (Bovine Serum Albumine) were administered subcutaneously in the backs of 6 weeks old female C57/BL6 mice (n=60, M1-M60, ref: SC-CJ-SS-F, Janvier Labs, France), anesthetized with isoflurane. Ten days after tumor cell implantation when tumours have reached sizes of 50 to 150 mm^3, mice were randomly separated into 6 groups (n=10 each) and treatment was started at day (D) 0, according to the protocols below. Experimental details are given in the supplementary material, tables S1 and S2. Briefly,

- Group 1 (M1 to M10) received M-PLL, followed by a series of 11 to 15 magnetic sessions (MS) at day (D) 0, D2, D4, D7, D9, D11, D14, D16, D18, D21, D23, D25, D28, D30, and D32. The applied alternating magnetic field (AMF) had a frequency of 198 kHz and a strength ranging from 11 to 27 mT during first MS and from 11 to 27 during subsequent MS.
- Group 2 (M11 to M20) received M-PLL without subsequent AMF application.
- Group 3 (M21 to M30) received IONPs, followed by a series of 7 to 15 MS at D0, D2, D4, D7, D9, D11, D14, D16, D18, D21, D23, D25, D28, D30, at D32. The applied AMF had a frequency of 198 Hz and a strength ranging from 22 to 31 mT during first MS and from 22 to 27 during subsequent MS.
- Group 4 (M31 to M40) received IONPs without subsequent AMF application.

In groups 1 to 4, M-PLL or IONPs were always administered at tumor centre at a quantity of 25 µg in iron per mm^3 of tumor (25 to 75 µL of nanoparticle suspensions at concentrations of 50 mg in iron per mL).

In groups 1 and 3, MS duration was always 30 minutes and the targeted intratumor temperature was 43-46°C. For the first MS, the targeted intratumor temperature was always reached while for subsequent MS it was not always the case, and the AMF was then set to a maximum strength of 27 mT. For mice in which tumor volumes exceeded 150% of initial tumor sizes and targeted temperature of 43-46 °C was not reached with a magnetic field frequency of 198 kHz and strength of 27 mT, a second intratumor nanoparticle administration at 25 µg in iron of nanoparticles per mm^3 of tumor was carried out.

- Group 5 (M41 to M50) received an intratumor administration of 50 µl of 5% glucose followed by a series of 4 to 10 MS at D0, D2, D4, D7, D9, D11, D14, D16, D18, D21. During each MS, an AMF of frequency 198 kHz and average strength 27 mT was applied.
- Group 6 (M51 to M60) received an intratumor administration of 50 µl of a suspension containing 5 % glucose.

Groups 2, 4, 5, and 6 are considered as control groups, *i.e.* groups of mice without nanoparticle administration and/or AMF applications.

Tumour volumes (TV), expressed in mm^3, were measured with a calliper and estimated using the formula $TV = 0.5.L.W^2$, where L and W are the largest and smallest tumor dimensions respectively, [34, 35]. Tumor volumes, mouse weight and mouse behaviour were either monitored or measured at D0, D2, D4, D7, D9, D11, D14, D16, D18, D21, D23, D25, D28, D30, D32. Mice were euthanized when tumor volumes exceeded 1000 mm^3 and/or when mice weight has decreased by more than 20 % from one measurement to the next one. Mouse survival curves were recorded during a 250 day period following first MS (D0).

Temperature monitoring and distribution

During each MS, intratumor temperature was first measured locally at the site of nanoparticle administration using an optical fibre (Fluoroptic Temperature Probe, LumaSense Technologies, France) placed in the central part of the tumour. Second, temperature distribution at tumour surface was also recorded using an Infrared Camera (EasIR-2, Optophase, France) positioned 20 cm above the coil. For infrared measurements, temperatures were measured along the X axis (parallel to the coil axis) and Y axis (perpendicular to the coil axis). During hyperthermia treatment each mouse is positioned similarly inside the coil and the spatial temperature distribution in X and Y directions are determined from the hottest point detected by the infrared camera, which is always positioned 20 cm above the coil. With this set-up we minimize the variations in measurement conditions between mice.

Specific absorption rates (SAR) of M-PLL and IONPs were measured in Watt per gram of iron, using the formula, $SAR = Cv.(\Delta T/\delta t).1/C_{Fe}$, where C_V = 4.2 J/(gK) is the specific heat capacity of water, $\Delta T/\delta t$, measured in C° per second, are the initial slopes of temperature variation with time, and C_{Fe}, measured in g of iron per g (mL) of water, is the concentration of nanoparticles. SAR was measured at tumor centre in mice of groups 1 and 3 during first MS using temperature measurements with the optical fibre. For the value of C_{Fe}, we used the concentration of the administered IONPs and M-PLL suspension, 25 mg

per mL of water, assuming that this corresponds to 25 µg per mm^3 of tumor. The method used for estimating the SAR *in vivo* is informative but would require further histological analysis to take into account in more details the nanoparticle distribution. In addition to the SAR, maximum temperature reached in the tumor and full width half maximum of the temperature distribution are also measured to be able to compare the heating efficacy between IONPs and M-PLL.

Statistics

Mouse survival rates are plotted using the Kaplan-Meier model method. Statistical significance of survival rate between the different groups is evaluated using the log rank test. Parameters are expressed as median and as p-values, as compared with control group 6, [36].

Histological analysis

For histological experiments, GL-261 subcutaneous tumors were grown in female C57/BL6 mice and treated under the same conditions than for thermotherapy treatments described above. Twelve mice were used for intratumoral injection of M-PLL (concentrations as above) in the presence (n=6) or not (n=6) of MS, 12 mice were used for intratumoral injection of IONPs (concentrations as above) in the presence (n=6) or not (n=6) of MS and 4 mice for the control conditions with glucose in the presence (n=2) or not (n=2) of MS. As before, MS included the application of a field of 10-32 mT and 198 kHz during 30 minutes in order to maintain an intratumoral temperature between 43 and 46°C. Half of the mice of each group were euthanized 6 hours after nanoparticle injection (one MS, if applicable) and the remaining mice were killed 72 hours after nanoparticle injection *i.e.* 24 hours after the second MS (two MS, if applicable). For all mice, subcutaneous tumors or skin were dissected, fixed in 4 % paraformaldehyde and embedded in paraffin. Sections of 4 µm were cut and stained with hematoxylin-eosin (H&E) or Perls Prussian Blue. Sections were imaged using an automated slide scanner (lamina, Perkin Elmer, USA).

Toxicity evaluation

Nanoparticle pyrogenicity was evaluated firstly by measuring the endotoxin concentration of the different nanoparticles using the Limulus amebocyte lysate (LAL) tests (Pierce LAL Chromogenic Endotoxin Quantitation Kit, Thermo Fisher Scientific, USA) and secondly by the rabbit test according to ISO10993-11.

Nanoparticle cytotoxicity was estimated for various nanoparticle and PLL concentrations (1000, 500, 125, 62.5, 31.25 or 15.62 µg/mL) on 3T3 (mouse fibroblast) cells using an MTT assay according to ISO 10993-5. Nanoparticles were considered as noncytotoxic for a percentage of cell inhibition below 30%. Nanoparticle cytotoxicity was also assessed on GL-261 cells using an MTT assay, following the same protocol as that used for 3T3 cells.

Nanoparticle acute systemic toxicity was evaluated according to ISO 10993-11. For that, C57/BL6 mice received 100 µL of M-PLL or IONPs (2 or 4 mg) intravenously. During the 10 days following injection, potential acute toxicity was evaluated by monitoring mouse body weight and behaviour.

More detailed information regarding nanoparticle toxicity evaluation is provided in the supplementary material section.

Results and Discussion

Categorization of M-PLL and IONPs

M-PLL and IONPs were both categorized as medical devices of class III according to European regulation (2007/47/EC) since the main mechanism of tumor destruction using these nanoparticles exposed to AMF is due to heat, i.e. antitumor activity was not observed for nanoparticles administered to tumors without AMF application. ISO 10993 international standards, which describe biological evaluation methods for medical devices that need to used according to drug agencies, were therefore followed.

Properties of M-PLL

Magnetosomes contained within whole magnetotactic bacteria, shown in Figure 1, or directly extracted from these bacteria without any specific treatments have been extensively studied due to their interesting properties such as high magnetization and chain arrangement, [37,38,39]. However, they cannot be used as such for biomedical application due to too high endotoxin concentrations, lying between 8.10^{+3} and 1.10^{+5} EU/mL/mg, as measured with LAL test.

We have therefore established a method for the fabrication of pyrogen-free magnetosomes that are biocompatible. For that, magnetosomes are first extracted from MSR-1 magnetotactic bacteria (Figures 1a and 1b) and purified (Figures 1c and 1d) to remove potentially toxic uncharacterized organic and pyrogenic materials surrounding the magnetosome minerals, leading to suspensions of magnetosome minerals, designated as M, with endotoxin concentrations between 10 and 100 EU/mL/mg, comparable to that of 50 EU/mL/mg measured for IONPs yet derived from chemical synthesis and thus normally exempt of endotoxins, [40]. Endotoxins are mostly removed in these suspensions but a

subsequent treatment is indeed necessary because M strongly aggregate. Indeed, absorbance measured at 480 nm of a suspension containing M decreases by more than 80 % in 10 minutes (Figure S1). Furthermore, TEM images of M, presented in Figures 1c and 1d, show aggregated magnetosomes minerals. For medical applications, aggregation should be avoided since it prevents a thorough administration and can induce adverse effect such as embolism.

To prevent their aggregation and enable their administration, M have therefore been coated with a polycationic polymer, PLL leading to M-PLL, [41]. TEM images of M-PLL, presented in Figures 1e and 1f, show a majority of coated magnetosomes of average sizes 40.5 ± 8.5 nm (Table S3 and Figure S2), with a majority organized in chains and a minority forming small aggregates. Composition of the magnetosome mineral core is determined to be maghemite using saturating isothermal remanent magnetization (Figure S3c), yielding saturating magnetization, Ms, and coercivity, Hc, values of 70 Am^2/Kg and 6 mT, respectively (Table S3). The presence of a coating surrounding the core in M-PLL is first revealed by the TEM image of Figure 1f, which shows a coating layer of 4 to 17 nm thickness (Table S3). In addition to the peaks at 609 and 673 cm^{-1}, due to iron oxide and also observed in the FT-IR spectrum of M (Figure S4a), the FT-IR spectrum of M-PLL (Figure S4a) reveals the presence of bands at 1546 cm^{-1} and 1656 cm^{-1}, which are attributed to NH and C=O compounds of amide functional groups contained in PLL, [42,43]. Second, CHNS analysis of M-PLL indicates 4.9% of carbon and 1.1 % of nitrogen (Table S3), which are higher values than those measured for M, suggesting the presence of organic material in M-PLL (Figure S4c). Third, zeta potential of M-PLL is positive over a wider range of pH for M-PLL ($2 < pH < 8$) than for M ($pH = 2$) (Figure S4b), which is indicative of a positively charged material within the coating at the surface of M-PLL. Moreover, M-PLL suspensions are nonpyrogenic, *i.e.* their endotoxin concentration is 80 EU/mg/mL and they pass the rabbit test carried out according to ISO 10993-11 (Supplementary Material). They are also considered as non-cytotoxic

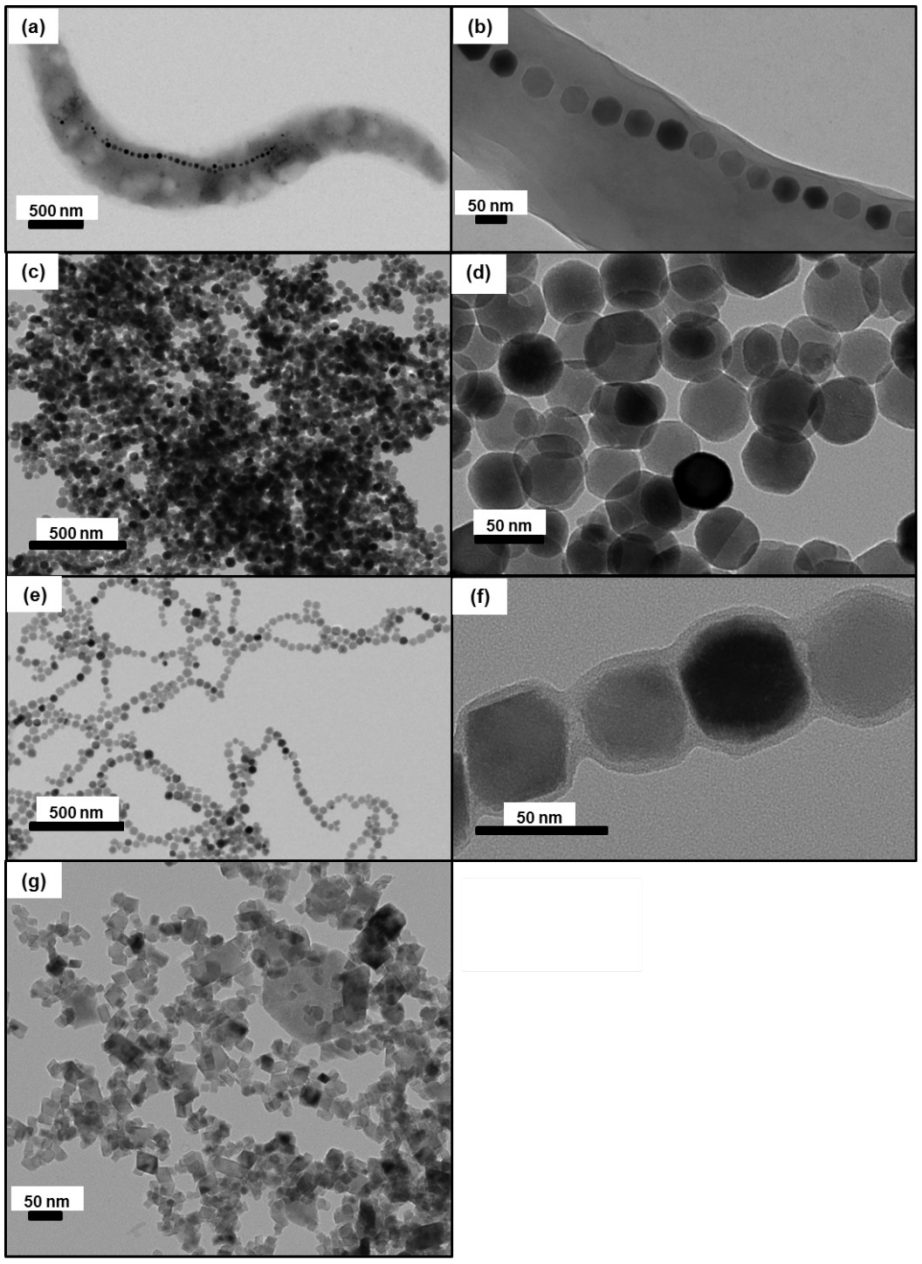

Figure 1. TEM images of, (a), an intact MSR-1 magnetotactic bacterium with intracellular chains of magnetosomes, (b), enlargement of the bacterium shown in (a), (c), aggregated uncoated magnetosome minerals, (d), enlargement of (c), (e), magnetosome minerals coated with poly-L-lysine forming chains and small aggregates, (f), enlargement of (e) showing a chain of magnetosomes coated with poly-L-lysine, (g) dispersed IONPs. For these observations, 5 µl of suspensions containing whole bacteria, uncoated magnetosomes, magnetosome minerals coated with poly-L-lysine and IONPs are deposited and dried on a carbon grid and then observed by TEM.

according to the criteria of ISO 10993-5, (Supplementary Material and Figure S5), [44]. M-PLL in suspensions are also shown to be sufficiently stable to enable their administration since the absorbance of this suspension, measured at 480 nm, decreases by less than 20 % in 15 minutes (Figure S1). Acute systemic toxicity of M-PLL, evaluated according to ISO 10993-11, by administering intravenously 100 µl of a M-PLL suspension of 25 or 50 mg of iron in M-PLL per ml in the tails of 6 weeks old C57/BL6 female mice indicate that the maximum tolerated dose (MTD) is larger than 4 mg (Figure S6). This result agrees with a previous study, reporting low magnetosome acute toxicity with LD_{50} of 15 mg/kg in rats, [45]. Furthermore, MTD of M-PLL is sufficiently high to enable treatment since it is much above 0.5 g, the amount of nanoparticles currently administered to human glioma of 15 cm^3 treated with magnetic hyperthermia, [46,47].

Properties of IONPs

IONPs are composed of an iron oxide core surrounded by hydroxy-methyl-starch as confirmed by the FT-IR spectrum of IONPs that shows three dominant bands attributed on the one hand to iron oxide at 607 cm^{-1} and on the other hand to Starch polymer at 1022 cm^{-1} and 1150 cm^{-1} (Figure S4a). They have a rectangular shape, an average size of 17 ± 4 (width) to 20 ± 5 (length) nm (Table S3), smaller than M-PLL, an organization in well dispersed small aggregates that differ from M-PLL chain arrangement, as observed in the TEM image of Figure 1g. This leads to Ms of 47 Am^2/kg and to Hc of 11 mT in agreement with previously published data, [48]. Compared with M-PLL, they appear to be less positively charged, + 5 mV at pH 7 (Figure S4b). They are stable in suspension (Figure S1) and biocompatible since they are nonpyrogenic, they are non-cytotoxic according to ISO 10993-5 (Figures S5a and S6) and characterized by a MTD larger than 4 mg.

Comparison between *in vivo* distribution of M-PLL and IONPs following the different magnetic sessions, deduced from temperature measurements and histological analysis

Previous studies have suggested to combine magnetic hyperthermia with MRI to determine iron oxide nanoparticle distribution in tumors during treatments, [49,50]. Under typical conditions applicable to magnetic hyperthermia treatment, *i.e.* following administration of 20 µl of magnetosomes at a concentration of 20 mg/mL at the center of intracranial RG-2 glioblastoma rat tumor of ~ 25 mm^3 and application of an AMF of 198 kHz and 20 mT for 20 minutes, the MRI scan of the tumor (Figure S7) shows a dense dark area revealing the presence of concentrated magnetosomes. This indicates that magnetosomes, which are known to be efficient contrast agents, [51,52], can be imaged with MRI. However, from a clinical perspective, we are not certain that MRI could be used during the various magnetic sessions since a too large magnetosome concentration can hide the tumor, as observed in Figure S7, and an induction system generating an AMF can hardly be introduced in or combined with MRI since both equipments generate different magnetic fields. In fact, MRI may either be used before treatment to identify tumor location and possibly guide magnetosome injection or after treatment to follow tumor growth evolution or ensure that the tumor has disappeared. During the various magnetic sessions, although invasive a temperature measurement method such as that presented in this study seems more suitable than MRI to detect the presence of magnetosomes and determine their distribution.

Nanoparticle temperature distribution is studied by administering 25 to 75 µl of a suspension containing M-PLL or IONPs at a concentration of 25 µg of iron per mm^3 of tumor once or twice at the centre of GL-261 glioma tumors of volumes of 50 to 150 mm^3 followed by 7 to 15 MS. We try to maintain intratumor temperature at 43-46 °C during the various MS by using, if necessary, a second intratumor nanoparticle administration and by adjusting the strength of the applied alternating magnetic field at 11 to 31 mT. Treatment parameters necessary to reach 43-46°C are used to compare nanoparticle and temperature distribution between M-PLL and IONPs.

During the first MS, temperatures between 43 and 46°C, measured 10 minutes following AMF application, are distributed within 3 mm (~ 100 mm^3) surrounding the tumour for M-PLL (Figure 2c) compared with 2 mm (~ 30 mm^3) for IONPs (Figure 2d). From these observations, mild hyperthermia (between 43 and 46°C) occurs within 100% of the tumor volume for M-PLL compared with less than 50% for IONPs (Figures 2c and 2d). We attribute these heating behaviors to higher heating capacity for M-PLL compared with IONPs. Indeed, the average SAR measured among 10 mice, deduced from the initial slopes of the temperature variations with time, $\Delta T/\delta t$ = 0.2 °C/sec. and $\Delta T/\delta t$ = 0.15 °C/sec., and from C_{Fe} = 25 µg per mm^3 of tumor, which is the estimated concentration of nanoparticles in the tumor, are 40 W/gFe and 26 W/gFe, for M-PLL and IONPs respectively (Figures 2a and 2b and Table S1). Moreover, the magnetic field strength necessary to reach 43-46°C is lower for M-PLL (11 to 27 mT) than for IONPs (22 to 31 mT).

Concerning temperature measurements carried out during subsequent MS, it appears that the numbers of sessions, without nanoparticle re-administration, during which 50% of mice reached tumor temperatures of 43-46 °C are 3 and 1 for M-PLL and IONPs, respectively, suggesting that the average time during which nanoparticles remain in sufficient quantity to heat the tumor is longer for M-PLL (5 days) than for IONPs (1 day).

While temperature, at 43-46 °C during the first MS, is distributed within a larger percentage of tumor volume for M-PLL than for IONPs, nanoparticle biodistribution, determined by optical microscopy analysis of tumor samples stained with H&E and Perls Prussian Blue reveals a very different behavior. Indeed, for samples collected 6 or 72 hours after nanoparticle administration without MS or followed by one or two MS, dense dark areas attributed to concentrated M-PLL are observed (Figures 3a, 3b, S8 and S9). In striking contrast, for mice treated in the same conditions but receiving IONPs instead of M-PLL, IONPs are less aggregated than M-PLL and are more homogenously dispersed (Figures 5, S10 and S11). On the one hand, these behaviors suggest that the more homogenous temperature distribution observed with M-PLL is not due to more homogenous nanoparticle distribution, but instead to a higher SAR value for M-PLL than for IONPs. On the other hand, the fact that M-PLL heat the tumor for a longer period than IONPs may come from different cellular interaction properties between the two types of nanoparticles. Indeed, as observed in Figure 4c, IONPs are localized at the same position as cells suggesting that they are internalized *in vivo*, possibly leading to nanoparticle degradation, which can undermine their heating properties. Recent works have shown that, when IONPs are internalized into cells their heating properties are significantly lowered by 70 to 90 %, [53,54].

By contrast, as observed in Figure 3c, M-PLL are aggregated and seem to concentrate mainly between cells, which could better preserve their heating properties compared with IONPs. These differences in behaviour, observed between M-PLL and IONPs, could be attributed to differences in charge at tumor pH of 6 (24 mV for M-PLL compared with 7 mV for IONP), organization (chains containing more 6 magnetosomes of size 40.5±8.5 nm for M-PLL versus single nanoparticle of average size 18.5±9 nm for IONPs), and magnetic properties (Ms ~ 70 Am²/Kg for M-PLL compared with Ms ~ 47 Am²/Kg for IONPs) as summarized in Table S3.

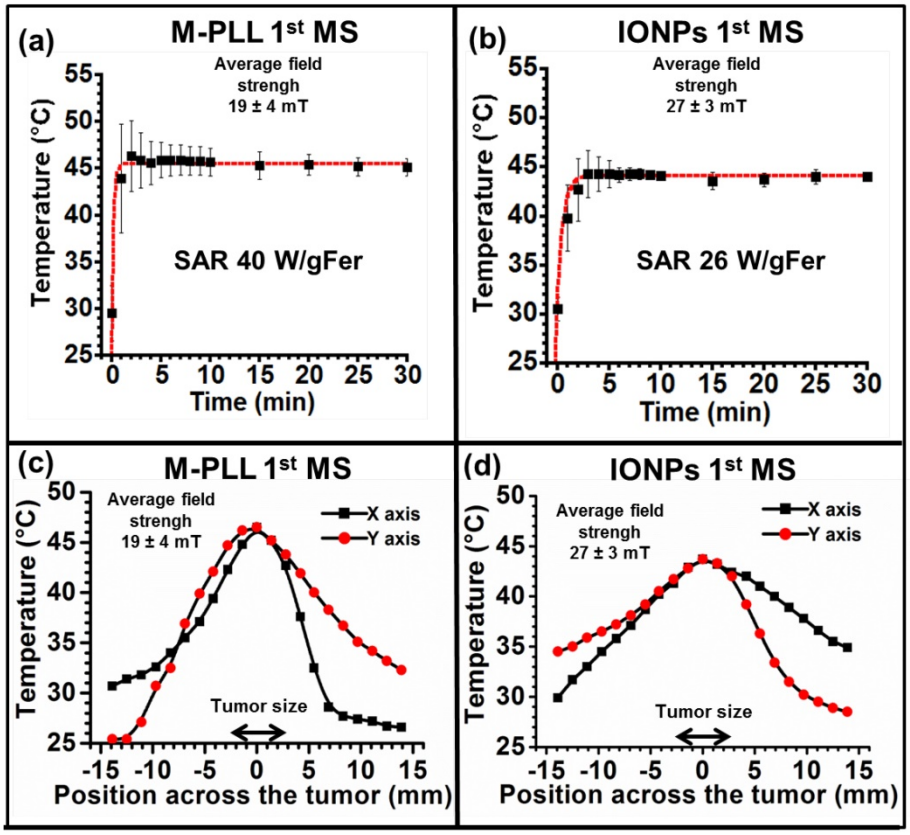

Figure 2. Temperature increases, measured at tumor center with an optical fibre during the first MS for mice belonging to group 1, (a), or to group 3, (b). The error bar reflects temperature differences measured between the various mice. Spatial infrared temperature distribution, measured at the skin surface along the coil axis, X, or perpendicular to this axis, Y, with an infrared camera 10 minutes after the beginning of the first MS for mice belonging to group 1, (c), or for those belonging to group 3, (d).

Comparison between *in vivo* antitumor efficacy of M-PLL and IONPs suspensions administered to GL-261 subcutaneous glioma tumors exposed to 7 to 15 MS

To compare the antitumor efficacy of IONPs with that of M-PLL, 6 groups (n=10) are treated under the following conditions: mice receive intratumorally M-PLL followed by 11 to 15 MS (group 1) or without MS (group 2); mice receive intratumorally IONPs followed by 7 to 15 MS (group 3) or without MS (group 4); mice are injected with glucose followed by 4 to 10 MS (group 5) or without MS (group 6).

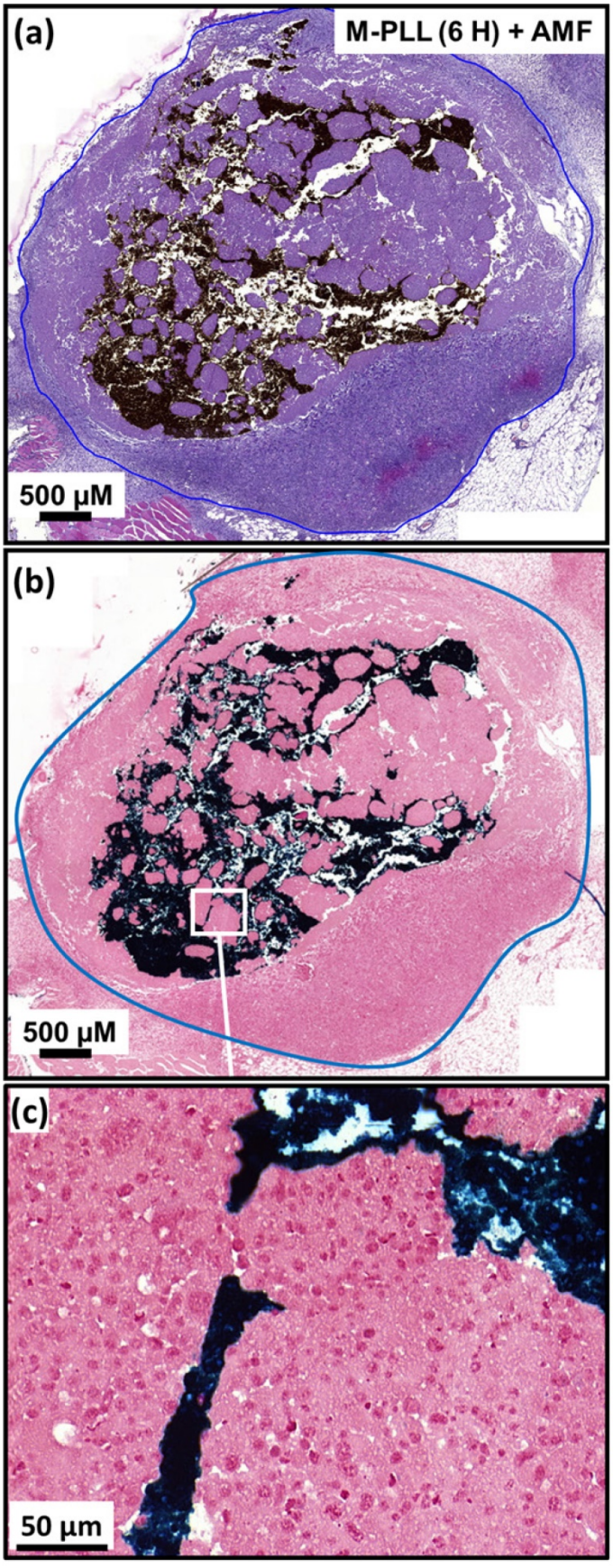

Figure 3. (a), H&E and (b), Perls Prussian blue section of a subcutaneous GL-261 tumor (blue circles) injected with 25 µg in iron of M-PLL per mm³ of tumor and collected 6 hours after the first MS (M-PLL (6H) + AMF). (c), enlargement of (b).

Anti-tumor effects are strong for mice belonging to group 1. Indeed, Figure 5a shows that tumor fully disappears among 5 mice at D2 (M1), D25 (M2), D7 (M5), D7 (M8) and D11 (M9) and that tumor growth is delayed among the remaining 5 mice (M3, M4, M6, M7, M10). Compared with control groups (groups 2, 5 and 6), in which tumor volumes increase continuously without any sign of anti-tumor activity (Figures 5b, 5f and 5e), leading to median survival time of 10 to 15 days, mice receiving M-PLL followed by 11 to 15 MS (group 1) are found to have much longer median survival times of 147 days ($p<0.0001$), (Figure 6 and Table S4). For a typical cured mouse without M-PLL re-administration (M8), photographs of tumors show that following 6 MS the tumor volume was considerably lower at day 11 (Figure 7b) than at day 0 (Figure 7a) and that a crust had developed (Figures 7b). In this mouse, after 12 MS at day 25 the tumor has fully disappeared and a scar is observed at the initial tumor location (Figure 7c). At day 250, neither tumor regrowth nor scar is observed (Figure 7d). Furthermore, a histological section of skin collected at day 250 in the former tumor region shows the absence of tumor cells, of M-PLL or of any sign of fibrosis resulting from tissue regeneration (Figure 7e). To further examine the effect of the treatment on tissues surrounding the tumor, tissue is collected from and near a tumor having received M-PLL followed by two MS. In Figures S8e and S8f, few necrotic areas are observed outside of the tumor, essentially located in the surrounding skin, which is a sign of inflammation associated with the presence of a crust. No necrotic areas are observed in fatty or muscle tissues, suggesting that the treatment did not induce any significant damage to healthy tissues surrounding the tumor (Figure S9e). These observations indicate that treatment is very well tolerated generating no observable adverse effects. Furthermore, following treatments, M-PLL seem to be progressively removed from the initial tumor region. Indeed, at day 250, M-PLL are not observed in this region but instead inside macrophages in lymph nodes (Figure 8), suggesting M-PLL elimination by macrophages. In mice belonging to group 1, in which the M-PLL suspension was re-administered at day 11 (M10), D14 (M3),

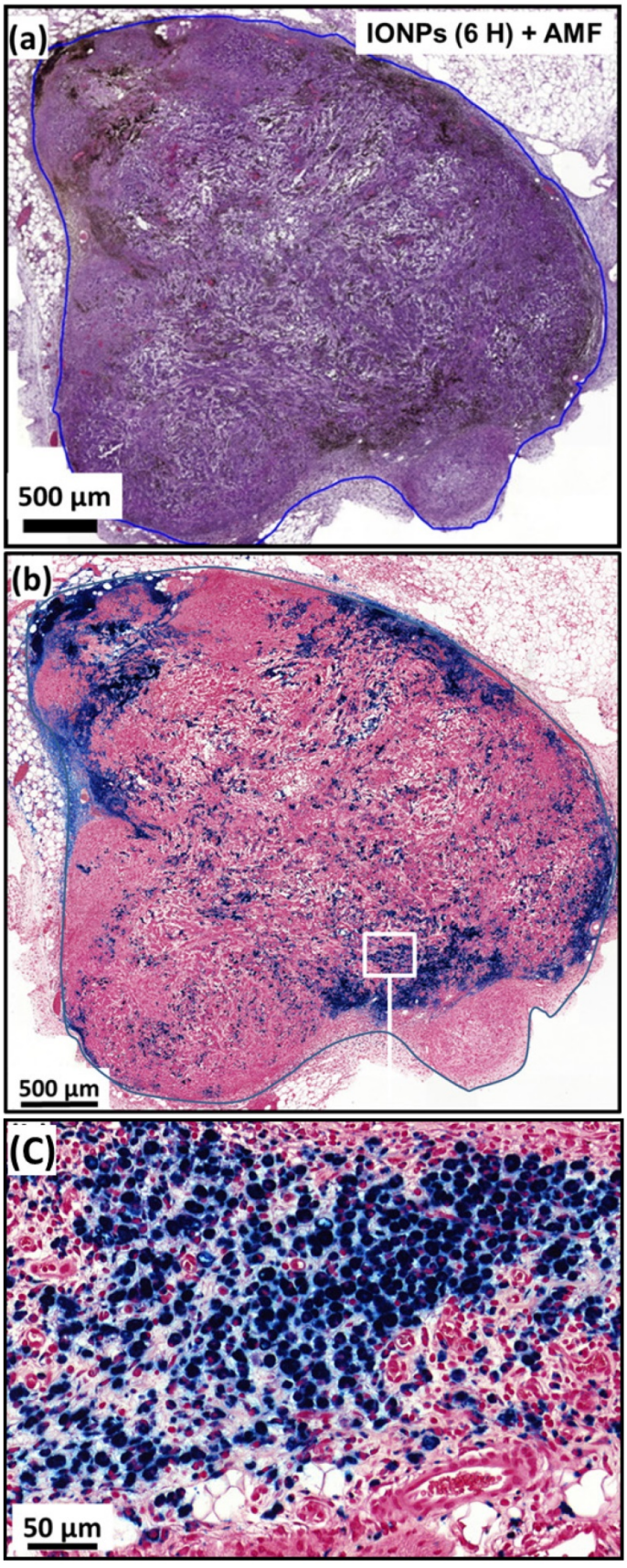

Figure 4. (a), H&E and (b), Perls Prussian blue section of a subcutaneous GL-261 tumor (blue circles) injected with 25 µg in iron of IONPs per mm³ of tumor and collected 6 hours after the first MS (IONPs (6H) + AMF). (c), enlargement of (b).

D16 (M7) and D18 (M4), due to tumor volume exceeding 150% of initial tumor volume at day 0, a decrease in tumor volume is observed during the days following re-administration without leading to full tumor disappearance (Figure 5). It shows that nanoparticle re-administration can be used to re-induce antitumor activity when the latter cannot anymore be achieved by increasing the magnetic field strength.

Anti-tumor activity is also observed among mice receiving IONPs followed by 7 to 15 MS (group 3) but is less pronounced. Indeed, tumor growth is delayed among 4 mice (M24, M26, M27, M29) and tumor disappears fully among 2 other mice at days 14 and 23 (M28, M30) as shown in Figures 5c and Figure 6. Compared with group 1 treated by M-PLL administration followed by 11 to 15 MS, mice receiving IONPs followed by 7 to 15 MS are characterized by a much shorter median survival time of 24 days ($p<0.0001$) (Table S5).

On the one hand, magnetic hyperthermia appears to be less safe with IONPs than with M-PLL since magnetic fields of higher strengths are required with IONPs (27 mT during first and subsequent MS) than with M-PLL (19 mT and 24 mT during first and subsequent MS, respectively) to yield anti-tumor efficacy. On the other hand, the longer residence time and the longer time at a temperature between 43-46 °C, for M-PLL, may be attributed to more localized concentrated nanoparticles and to a higher SAR value. This leads to enhanced antitumor activity with M-PLL, possibly by promoting: i), vascular injury leading to tumor ischaemia, [55], ii), an immune response, possibly induced by activated stressed proteins such as heat shock proteins (HSP), [56, 57], iii), an apoptotic cell death mechanism, [58].

Compared with previous preclinical studies showing increased survival by 15-44 days of rats bearing RG-2 or T-9 glioma tumors and treated by magnetic hyperthermia at 43-47 °C, [59,60], our study reports for the first-time full cure of subcutaneous GL-261 tumors in a significant percentage of mice (50%) using biocompatible nanoparticles synthesized biologically by magnetotactic bacteria with improved properties, compared with previously used chemically synthesized nanoparticles.

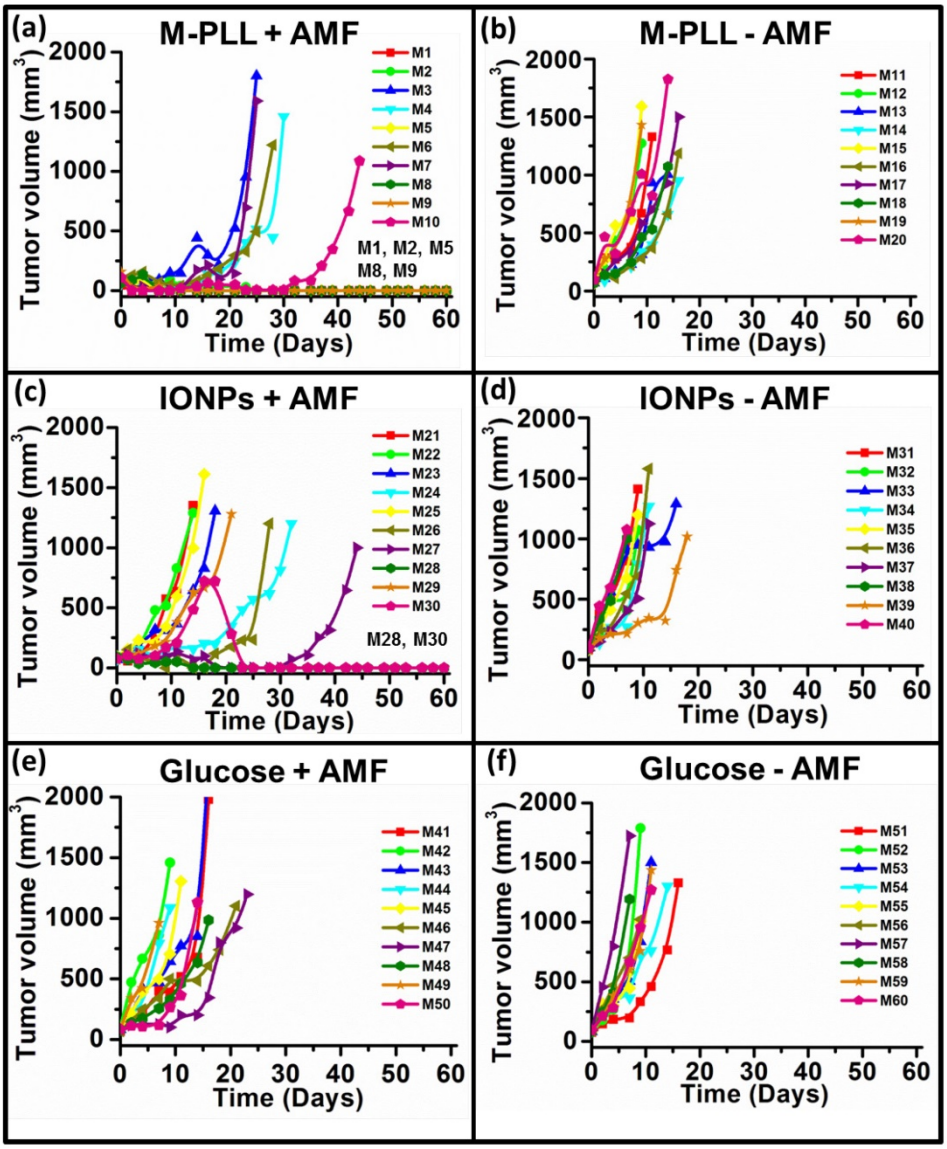

Figure 5. Tumor volume variation as a function of time following administration of glucose, M-PLL or IONPs for mice belonging to group 1, (a), group 2, (b), group 3, (c), group 4, (d), group 5, (e), group 6, (f). Each mouse is designated by a number in each figure.

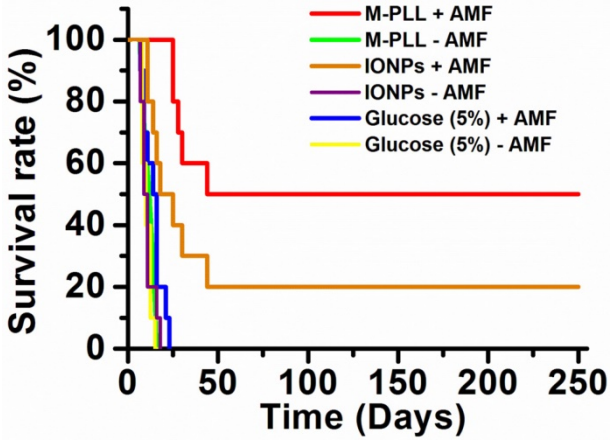

Figure 6. Survival rate of mice belonging to group 1 (M-PLL+AMF), group 2 (M-PLL-AMF), group 3 (IONPs+AMF), group 4 (IONPs-AMF), group 5 (Glucose (5%)+AMF), and group 6 (Glucose (5%)-AMF).

Conclusion

In summary, we present a method to fabricate pyrogen free biocompatible magnetosomes synthesized by magnetotatic bacteria. For that, magnetosomes are purified to remove bacterial residues and magnetosome minerals are stabilized with a poly-L-lysine coating to yield M-PLL. When M-PLL are administered to rats and mice, they are shown to be excellent MRI contrast agents, and to lead to 50% of mice fully cured 5 weeks following M-PLL administration and several applications of a safe AMF, *i.e.* characterized by H.f = 2-4 10^8 $A.m^{-1}.s^{-1}$, well below the threshold of 5.10^9 $A.m^{-1}.s^{-1}$ above which eddy currents may occur, [61]. Enhanced M-PLL efficacy compared with IONPs is attributed to a higher SAR value, *i.e.* SAR of 40 W/gFe and 26 W/gFe

are estimated for M-PLL and IONP, respectively, and to a longer residence time in tumors, *i.e.* 5 and 1 day(s) for M-PLL and IONPs, respectively, which result in temperatures between 43 and 46 °C being more homogenously distributed within the whole tumor and being reached over a longer period of time without nanoparticle re-administration. Interestingly, improved M-PLL efficacy is obtained while tumor coverage is partial and nanoparticles are less dispersed. The mechanisms by which tumor without M-PLL or containing a low M-PLL quantity are destroyed upon application of an AMF may involve tumor ischemia and/or enhancement of the antitumor immune response.

This study complements previous works, which showed that magnetosomes could be used in a range of different medical applications, (62), including diagnosis, (63), and cancer treatment, (64-67).

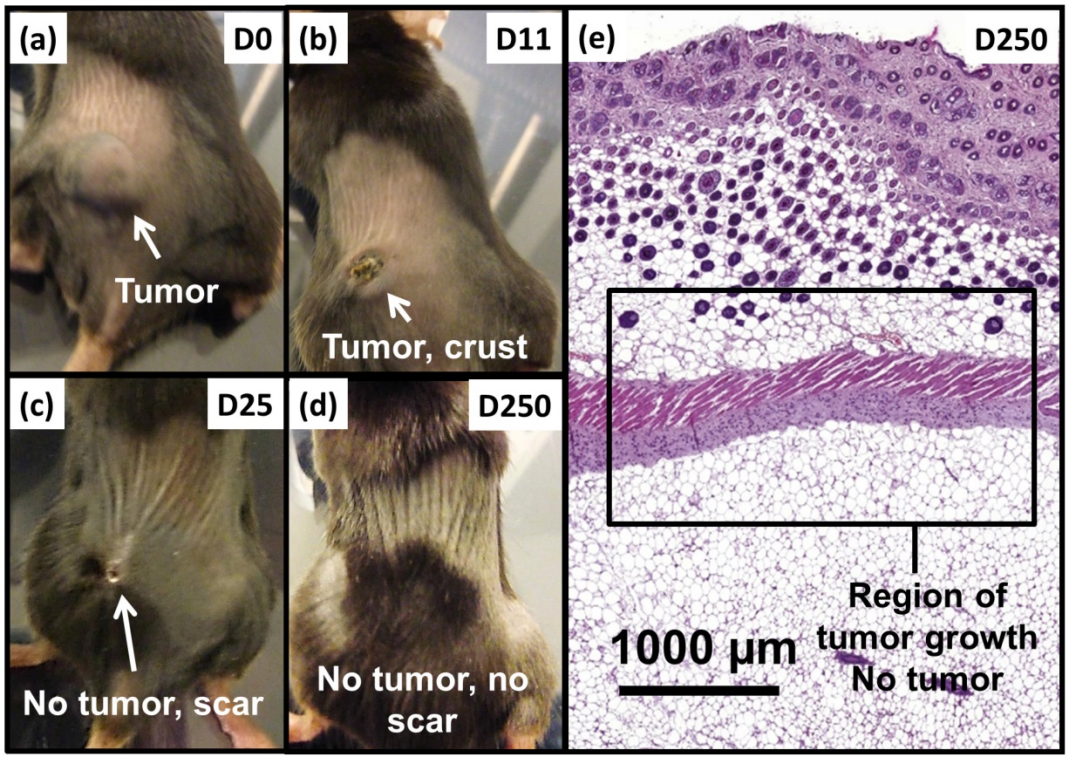

Figure 7. Photographs of a typical mouse following M-PLL injection belonging to group 1 showing, (a), a large tumor at D0, (b), a small tumor and a crust at D11, (c), the absence of tumor and a scar at D25 and (d), the absence of tumor and scar at D250. (e), H&E section of skin collected at D250 in region of initial tumor location showing the absence of tumor.

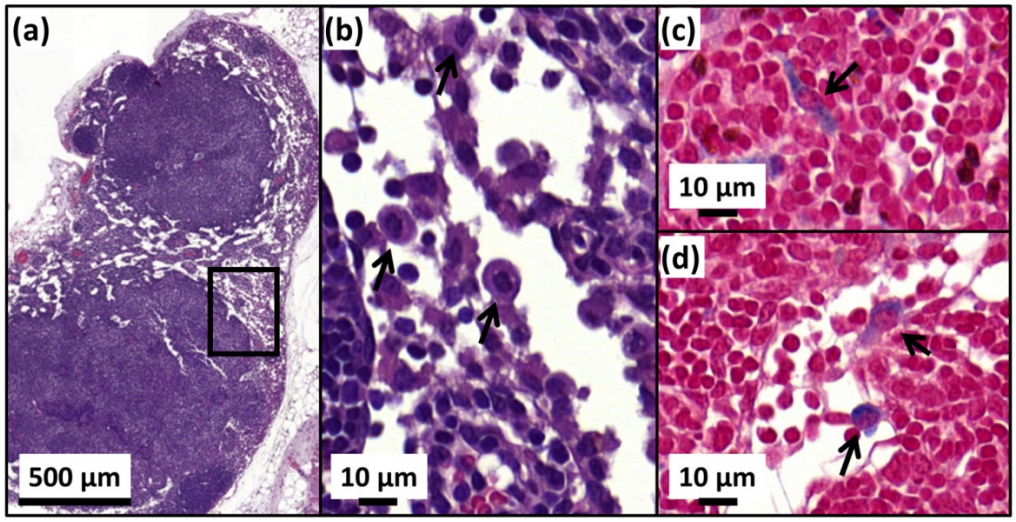

Figure 8. H&E (a,b) and Perls Prussian blue (c,d) sections of a lymph node in the skin of a cured mice treated with 25 µg in iron of M-PLL per mm³ of tumor followed by 15 MS and collected at D250. (a), the whole lymph node. (b), an enlargement of (a) showing macrophages (black arrows). (c) and (d), enlargements of (a) showing blue coloration in the cytoplasm of macrophages (black arrows) suggesting the elimination of M-PLL from the region of initial tumor location by macrophages.

Acknowledgments

We would like to thank the Eurostars program (Nanoneck-2, E9309), subvention AIR from the region of Paris (A1401025Q) as well as the ANRT (CIFRE 2013/0364 between Nanobacterie and palaeomagnetism laboratory at ''*Institut de Physique du Globe de Paris*'', CIFRE 2014/0359 between Nanobacterie and the ''*Muséum d'histoire naturelle*''), the ANR Méfisto. Raphaël Le Fèvre is a PhD student, working both at Nanobacterie and at the IPGP. Most of the experiments presented in this study, except magnetic measurements, were carried out in Nanobacterie Laboratory. Experiments were carried out by Raphaël Le Fèvre under general supervision of Edouard Alphandéry, with the help of Mickaël Durand-Dubief and Chalani Mandawala for nanoparticle preparation, Imène chebbi and Mickaël Durand-Dubief regarding *in vitro* and *in vivo* studies, Imène Chebbi, Caroline Maake, Clovis Adam, and the platform 'Histim' of the Cochin Institute concerning histological experiments. The writing of the article and analysis of the results were mainly carried out by Edouard Alphandéry and Raphael Le Fèvre, with the help of François Guyot, Caroline Maake, France Lagroix and Jean-Pierre Valet. Jean-Yves Delattre, Ahmed Idbaih, and Charlotte Schmitt commented on relevance of the preclinical protocol to verify that it is clinically applicable since this group will be possibly be in charge of the clinical trials using this treatment. Magnetic measurements were carried out at the IPGP under the supervision of France Lagroix and Jean-Pierre Valet.

Other Information

Mickaël Durand-Dubief carried out the work presented in this study while he was working at Nanobacterie. He is currently working at the department of Biosciences and Nutrition, Karolinska Institutet Novum, 141 83 Huddinge, Sweden and can be contacted at this address.

Supplementary Material

Supplementary figures and tables.
http://www.thno.org/v07p4618s1.pdf

Competing Interests

The authors have declared that no competing interest exists.

References

1. Figuerola A, Di Corato R, Manna L, Pellegrino T. From iron oxide nanoparticles towards advanced iron-based inorganic materials designed for biomedical applications. Pharmacol Res. 2010; 62(2): 126-43.
2. Laurent S, Forge D, Port M, Roch A, Robic C, Vander Elst L, Muller RN. Magnetic iron oxide nanoparticles: synthesis, stabilization, vectorization, physicochemical characterizations, and biological applications. Chem Rev. 2008; 108(6): 2064-110.
3. Kumar CS, Mohammad F. Magnetic nanomaterials for hyperthermia-based therapy and controlled drug delivery. Adv Drug Deliv Rev. 2011; 63(9): 789-808.
4. Bañobre-López M, Teijeiro A, Rivas J. Magnetic nanoparticle-based hyperthermia for cancer treatment. Rep Pract Oncol Radiother. 2013; 18(6): 397-400.
5. Maier-Hauff K, Ulrich F, Nestler D, Niehoff H, Wust P, Thiesen B, Orawa H, Budach V, Jordan A. Efficacy and safety of intratumoral thermotherapy using magnetic iron-oxide nanoparticles combined with external beam radiotherapy on patients with recurrent glioblastoma multiforme. J Neurooncol. 2011; 103(2): 317-24.
6. Hanihara M, Kawataki T, Oh-Oka K, Mitsuka K, Nakao A, Kinouchi H. Synergistic antitumor effect with indoleamine 2,3-dioxygenase inhibition and temozolomide in a murine glioma model. J Neurosurg. 2016; 124(6): 1594-601.
7. Chakravarti A, Erkkinen MG, Nestler U, Stupp R, Mehta M, Aldape K, Gilbert MR, Black PM, Loeffler JS. Temozolomide-mediated radiation enhancement in glioblastoma: a report on underlying mechanisms. Clin Cancer Res. 2006; 12(15): 4738-46.
8. Stupp R, Mason WP, van den Bent MJ, Weller M, Fisher B, Taphoorn MJ, Belanger K, Brandes AA, Marosi C, Bogdahn U, Curschmann J, Janzer RC, Ludwin SK, Gorlia T, Allgeier A, Lacombe D, Cairncross JG, Eisenhauer E, Mirimanoff RO; European Organisation for Research and Treatment of Cancer Brain Tumor and Radiotherapy Groups; National Cancer Institute of Canada Clinical Trials Group. Radiotherapy plus concomitant and adjuvant temozolomide for glioblastoma. N Engl J Med. 2005; 352(10): 987-96.
9. Fine HA, Wen PY, Maher EA, Viscosi E, Batchelor T, Lakhani N, Figg WD, Purow BW, Borkowf CB. Phase II trial of thalidomide and carmustine for patients with recurrent high-grade gliomas. J Clin Oncol. 2003; 21(12): 2299-304.
10. Bennett CL, Angelotta C, Yarnold PR, Evens AM, Zonder JA, Raisch DW, Richardson P. Thalidomide- and lenalidomide-associated thromboembolism among patients with cancer. JAMA. 2006; 296(21): 2558-60.
11. Authier A, Farrand KJ, Broadley KW, Ancelet LR, Hunn MK, Stone S, McConnell MJ, Hermans IF. Enhanced immunosuppression by therapy-exposed glioblastoma multiforme tumor cells. Int J Cancer. 2015; 136(11): 2566-78.
12. Matsunaga T, Suzuki T, Tanaka M, Arakaki A. Molecular analysis of magnetotactic bacteria and development of functional bacterial magnetic particles for nano-biotechnology. Trends Biotechnol. 2007; 25(4): 182-8.
13. Araujo AC, Abreu F, Tavares Silva K, Bazylinski D, Lins U. Magnetotactic Bacteria as Potential Sources of Bioproducts. Mar Drugs. 2015; 13(1): 389–430.
14. Orlando T, Mannucci S, Fantechi E, Conti G, Tambalo S, Busato A, Innocenti C, Ghin L, Bassi R, Arosio P, Orsini F, Sangregorio C, Corti M, Casula MF, Marzola P, Lascialfari A, Sbarbati A. Characterization of magnetic nanoparticles from Magnetospirillum Gryphiswaldense as potential theranostics tools. Contrast Media Mol Imaging. 2016; 11(2): 139-45.
15. Ito A, Shinkai M, Honda H, Kobayashi T. Medical application of functionalized magnetic nanoparticles. J Biosci Bioeng. 2005; 100(1): 1-11.
16. Alphandéry E, Faure S, Seksek O, Guyot F, Chebbi I. Chains of magnetosomes extracted from AMB-1 magnetotactic bacteria for application in alternative magnetic field cancer therapy. ACS Nano. 2011; 5(8): 6279-96.
17. Alphandéry E, Amor M, Guyot F, Chebbi I. The effect of iron-chelating agents on Magnetospirillum magneticum strain AMB-1: stimulated growth and magnetosome production and improved magnetosome heating properties. Appl Microbiol Biotechnol. 2012; 96(3): 663-70.
18. Matsunaga T, Tadokoro F, Nakamura N. Mass culture of magnetic bacteria and their application to flow type immunoassays. IEEE Transactions on Magnetics. 1990; 26(5): 1557-59.
19. Yanase M, Shinkai M, Honda H, Wakabayashi T, Yoshida J, Kobayashi T. Intracellular hyperthermia for cancer using magnetite cationic liposomes: an in vivo study. Jpn J Cancer Res. 1998; 89(4): 463-9.
20. Suzuki M, Shinkai M, Honda H, Kobayashi T. Anticancer effect and immune induction by hyperthermia of malignant melanoma using magnetite cationic liposomes. Melanoma Res. 2003; 13(2): 129-35.
21. Tanaka K, Ito A, Kobayashi T, Kawamura T, Shimada S, Matsumoto K, Saida T, Honda H. Heat immunotherapy using magnetic nanoparticles and dendritic cells for T-lymphoma. J Biosci Bioeng. 2005; 100(1): 112-5.
22. Johannsen M, Thiesen B, Gneveckow U, Taymoorian K, Waldöfner N, Scholz R, Deger S, Jung K, Loening SA, Jordan A. Thermotherapy using magnetic nanoparticles combined with external radiation in an orthotopic rat model of prostate cancer. Prostate. 2006; 66(1): 97-104.
23. Toraya-Brown S, Sheen MR, Zhang P, Chen L, Baird JR, Demidenko E, Turk MJ, Hoopes PJ, Conejo-Garcia JR, Fiering S. Local hyperthermia treatment of tumors induces CD8 (+) T cell-mediated resistance against distal and secondary tumors. Nanomedicine. 2014; 10(6): 1273-85.
24. Zadnik PL, Molina CA, Sarabia-Estrada R, Groves ML, Wabler M, Mihalic J, McCarthy EF, Gokaslan ZL, Ivkov R, Sciubba D. Characterization of intratumor magnetic nanoparticle distribution and heating in a rat model of metastatic spine disease. J Neurosurg Spine. 2014; 20(6): 740-50.
25. Dennis CL, Jackson AJ, Borchers JA, Hoopes PJ, Strawbridge R, Foreman AR, van Lierop J, Grüttner C, Ivkov R. Nearly complete regression of tumors via collective behavior of magnetic nanoparticles in hyperthermia. Nanotechnology. 2009; 20(39): 395103.

26. Schultheiss D, Schüler D. Development of a genetic system for Magnetospirillum gryphiswaldense. Arch Microbiol. 2003; 179(2): 89-94.
27. Heyen U, Schüler D. Growth and magnetosome formation by microaerophilic Magnetospirillum strains in an oxygen-controlled fermentor. Appl Microbiol Biotechnol. 2003; 61(5-6): 536-44.
28. Zhang Y, Zhang X, Jiang W, Li Y, Li J. Semicontinuous culture of Magnetospirillum gryphiswaldense MSR-1 cells in an autofermentor by nutrient-balanced and isosmotic feeding strategies. Appl Environ Microbiol. 2011; 77(17): 5851-6.
29. Yang J, Li S, Huang X, Tang T, Jiang W, Zhang T, Li Y. A key time point for cell growth and magnetosome synthesis of Magnetospirillum gryphiswaldense based on real-time analysis of physiological factors. Front Microbiol. 2013; 4: 210.
30. Sun JB, Zhao F, Tang T, Jiang W, Tian JS, Li Y, Li JL. High-yield growth and magnetosome formation by Magnetospirillum gryphiswaldense MSR-1 in an oxygen-controlled fermentor supplied solely with air. Appl Microbiol Biotechnol. 2008; 79(3): 389-97.
31. Bordelon DE, Cornejo C, Grüttner C, Westphal F, DeWeese TL, Ivkov R. Magnetic nanoparticle heating efficiency reveals magneto-structural differences when characterized with wide ranging and high amplitude alternating magnetic fields. J. Appl. Phys. 2011; 109:124904.
32. Kekalo K, Baker I, Meyers R, Shyong J. Magnetic Nanoparticles with High Specific Absorption Rate at Low Alternating Magnetic Field. Nano Life. 2015; 5(2): 1550002.
33. Patent/US20150306246A1. Magnetic nanoparticles, composites, suspensions and colloids with high specific absorption rate (sar). Issued 6 December 2013.
34. Tomayko MM, Reynolds CP. Determination of subcutaneous tumor size in athymic (nude) mice. Cancer Chemother Pharmacol. 1989; 24(3): 148-54.
35. Ito A, Shinkai M, Honda H, Kobayashi T. Heat-inducible TNF-alpha gene therapy combined with hyperthermia using magnetic nanoparticles as a novel tumor targeted therapy. Cancer Gene Ther. 2001; 8(9): 649-54.
36. Heitjan DF, Manni A, Santen RJ. Statistical analysis of in vivo tumor growth experiments. Cancer Res. 1993; 53(24): 6042-50.
37. Lang C, Schüler D, Faivre D. Synthesis of magnetite nanoparticles for bio- and nanotechnology: genetic engineering and biomimetics of bacterial magnetosomes. Macromol Biosci. 2007; 7(2): 144-51.
38. Yan L, Zhang S, Chen P, Liu H, Yin H, Li H. Magnetotactic bacteria, magnetosomes and their application. Microbiol Res. 2012; 167(9): 507-19.
39. Staniland SS. Magnetosomes: Bacterial biosynthesis of magnetic nanoparticles and potential biomedical applications. In: Wiley-VCH. Magnetic nanomaterials. 2009: 399-430.
40. Andrade SS, Silveira RL, Schmidt C, Dalmora SL. Comparative evaluation of the human whole blood and human peripheral blood monocyte tests for pyrogens. International Journal of Pharmaceutics. 2004; 265(1-2): 115-24.
41. Wang X, Wei F, Liu A, Wang L, Wang JC, Ren L, Liu W, Tu Q, Li L, Wang J. Cancer stem cell labeling using poly (L-lysine)-modified iron oxide nanoparticles. Biomaterials. 2012; 33(14): 3719-32.
42. Rozenberg M, Shoham G. FTIR spectra of solid poly-l-lysine in the stretching NH mode range. Biophys Chem. 2007; 125(1): 166-71.
43. Tam SK, Dusseault J, Polizu S, Ménard M, Hallé JP, Yahia L. Physicochemical model of alginate-poly-L-lysine microcapsules defined at the micrometric/nanometric scale using ATR-FTIR, XPS, and ToF-SIMS. Biomaterials. 2005; 26(34): 6950-61.
44. ISO 10993-12:2007 - Biological Evaluation of Medical Devices -- Part 12: Sample Preparation and Reference Materials, ISO, accessed 21 November 2016.
45. Isaksson K, Akerberg D, Posaric-Bauden M, Andersson R, Tingstedt B. In vivo toxicity and biodistribution of intraperitoneal and intravenous poly-L-lysine and poly-L-lysine/poly-L-glutamate in rats. J Mater Sci Mater Med. 2014; 25(5): 1293-9.
46. Freireich EJ, Gehan EA, Rall DP, Schmidt LH, Skipper HE. Quantitative comparison of toxicity of anticancer agents in mouse, rat, hamster, dog, monkey, and man. Cancer Chemother Rep. 1966; 50(4): 219-44.
47. Maier-Hauff K, Rothe R, Scholz R, Gneveckow U, Wust P, Thiesen B, Feussner A, von Deimling A, Waldoefner N, Felix R, Jordan A. Intracranial thermotherapy using magnetic nanoparticles combined with external beam radiotherapy: results of a feasibility study on patients with glioblastoma multiforme. J Neurooncol. 2007; 81(1): 53-60.
48. Branquinho LC, Carrião MS, Costa AS, Zufelato N, Sousa MH, Miotto R, Ivkov R, Bakuzis AF. Effect of magnetic dipolar interactions on nanoparticle heating efficiency: implications for cancer hyperthermia. Sci Rep. 2013; 3: 2887.
49. Hayashi K, Nakamura M, Sakamoto W, Yogo T, Miki H, Ozaki S, Abe M, Matsumoto T, Ishimura K. Superparamagnetic nanoparticle clusters for cancer theranostics combining magnetic resonance imaging and hyperthermia treatment. Theranostics. 2013; 3(6): 366-76.
50. Zhao Q, Wang L, Cheng R, Mao L, Arnold RD, Howerth EW, Chen ZG, Platt S. Magnetic nanoparticle-based hyperthermia for head & neck cancer in mouse models. Theranostics. 2012; 2: 113-21.
51. Hu L ; Zhang F, Wang F, You XF, Nie L, Wang HX, Song T, Yang WH. Comparison of the 1H NMR Relaxation Enhancement Produced by Bacterial Magnetosomes and Synthetic Iron Oxide Nanoparticles for Potential Use as MR Molecular Probes. IEEE Transactions on Applied Superconductivity. 2011; 20(3): 822-825.
52. Lee N, Kim H, Choi SH, Park M, Kim D, Kim HC, Choi Y, Lin S, Kim BH, Jung HS, Kim H, Park KS, Moon WK, Hyeon T. Magnetosome-like ferrimagnetic iron oxide nanocubes for highly sensitive MRI of single cells and transplanted pancreatic islets. PNAS. 2011; 108(7): 2662-7.
53. Di Corato R, Espinosa A, Lartigue L, Tharaud M, Chat S, Pellegrino T, Ménager C, Gazeau F, Wilhelm C. Magnetic hyperthermia efficiency in the cellular environment for different nanoparticle designs. Biomaterials. 2014; 35(24): 6400-11.
54. Guardia P, Di Corato R, Lartigue L, Wilhelm C, Espinosa A, Garcia-Hernandez M, Gazeau F, Manna L, Pellegrino T. Water-soluble iron oxide nanocubes with high values of specific absorption rate for cancer cell hyperthermia treatment. ACS Nano. 2012; 6(4): 3080-91.
55. Chu KF, Dupuy DE. Thermal ablation of tumours: biological mechanisms and advances in therapy. Nat Rev Cancer. 2014; 14(3): 199-208.
56. Toraya-Brown S, Fiering S. Local tumour hyperthermia as immunotherapy for metastatic cancer. Int J Hyperthermia. 2014; 30(8): 531–539.
57. Ito A, Shinkai M, Honda H, Yoshikawa K, Saga S, Wakabayashi T, Yoshida J, Kobayashi T. Heat shock protein 70 expression induces antitumor immunity during intracellular hyperthermia using magnetite nanoparticles. Cancer Immunol Immunother. 2003; 52(2): 80-8.
58. Hall EJ. The bystander effect. Health Phys. 2003; 85(1): 31-5.
59. Jordan A, Scholz R, Maier-Hauff K, van Landeghem FK, Waldoefner N, Teichgraeber U, Pinkernelle J, Bruhn H, Neumann F, Thiesen B, von Deimling A, Felix R. The effect of thermotherapy using magnetic nanoparticles on rat malignant glioma. J Neurooncol. 2006; 78(1): 7-14.
60. Ohno T, Wakabayashi T, Takemura A, Yoshida J, Ito A, Shinkai M, Honda H, Kobayashi T. Effective solitary hyperthermia treatment of malignant glioma using stick type CMC-magnetite. In vivo study. J Neurooncol. 2002; 56(3): 233-9.
61. Dutz S, Hergt R. Magnetic nanoparticle heating and heat transfer on a microscale: Basic principles, realities and physical limitations of hyperthermia for tumour therapy. Int J Hyperthermia. 2013; 29(8): 790-800.
62. Alphandéry E, Grand-Dewyse P, Le Fèvre R, Mandawala C, Durand-Dubief M. Cancer therapy using nanoformulated substances: scientific, regulatory and financial aspects. Expert Review of anticancer therapy. 2015; 15(10): 1233-1255.
63. Alphandéry E, Lijeour L, Lalatonne Y, Motte L. Different signatures between chemically and biologically synthesized nanoparticles in a magnetic sensor: A new technology for multiparametric detection. Sensors and Actuators B. 2010; 147: 786-790.
64. Alphandéry E, Idbaih A, Adam C, Delattre J-Y, Schmitt C, Guyot F, Chebbi I. Chains of magnetosomes with controlled endotoxin release and partial tumor occupation induce full tumor destruction of intracranial U87-Luc glioma in mice under the application of an alternating magnetic field. Journal of controlled release. 2017; 262: 259-272.
65. Alphandéry E, Idbaih A, Adam C, Delattre J-Y, Schmitt C, Guyot F, Chebbi I. Development of non-pyrogenic magnetosome minerals coated with poly-l-lysine leading to full disappearance of incranial U87-Luc glioblastoma in 100% of treated mice using magnetic hyperthermia. Biomaterials. 2017; 141: 210-222.
66. Mandawala C, Chebbi I, Durand-Dubief M, Le Fèvre R, Hamdous Y, Guyot F, Alphandéry E. Biocompatible and stable magnetosome minerals coated with poly-l-lysine, citric acid, and carboxy-methyl-dextran for application in the magnetic hyperthermia treatment of tumors. Journal of Materials Chemistry B. 2017. DOI: 10.1039/c6tb03248f
67. Hamdous Y, Chebbi I, Mandawala C, Le Fèvre R, Guyot F, Seksek O, Alphandéry E. Biocompatible coated magnetosome minerals with various organization and cellular interaction properties induce cytotoxicity towards RG-2 and GL-261 glioma cells in the presence of an alternating magnetic field. Journal of nanobiotchnlogy. 2017. DOI: 10.1186/s12951-017-0293-2.